Mon. Not. R. Astron. Soc. **000**, 000–000 (0000) Printed 1 February 2008 (MN LATEX style file v1.4)

CMB anisotropy: deviations from Gaussianity due to non-linear gravity

A.M. Aliaga[1], V. Quilis[2], J.V. Arnau[3] & D. Sáez[1,4]
[1] *Departamento de Astronomía y Astrofísica, Universidad de Valencia. 46100 Burjassot, Valencia, Spain*
[2] *Department of Physics, Durham University, South Road, Durham, DH1 3LE, UK*
[3] *Departamento de Matemática Aplicada, Universidad de Valencia. 46100 Burjassot, Valencia, Spain*
[4] *email:diego.saez@uv.es*

1 February 2008

ABSTRACT
Non-linear evolution of cosmological energy density fluctuations triggers deviations from Gaussianity in the temperature distribution of the cosmic microwave background. A method to estimate these deviations is proposed. N-body simulations – in a ΛCDM cosmology – are used to simulate the strongly non-linear evolution of cosmological structures. It is proved that these simulations can be combined with the potential approximation to calculate the statistical moments of the CMB anisotropies produced by non-linear gravity. Some of these moments are computed and the resulting values are different from those corresponding to Gaussianity.

Key words: cosmic microwave background—cosmology:theory— large-scale structure of the universe.

1 INTRODUCTION

Many experiments have been designed to analyze the Cosmic Microwave Background (CMB) anisotropy. The signal to be detected is the superposition of various components. In the inflationary models considered here, the components generated during linear evolution (Sachs-Wolfe, Doppler, and so on) are dominant and Gaussian; nevertheless, there are subdominant non Gaussian components as those due to non-linear gravity (Rees-Sciama), lens distortions, and contaminant foregrounds. The characterization of all these subdominant components, including deviations with respect to Gaussianity, is necessary for data analysis in experiments as MAP and PLANCK. The Rees-Sciama effect was studied, using N-body simulations, by Seljak (1996) and Tuluie, Laguna & Anninos (1996); nevertheless, deviations with respect to Gaussianity were not considered at all by these authors. The third order moment of the Rees-Sciama effect was estimated, using second order perturbation theory (not a fully non-linear method describing strongly non-linear evolution), by Mollerach et al. (1995) and Munshi, Souradeep & Starobinski (1995). Here, we are mainly concerned with the deviations with respect to Gaussianity produced by fully non-linear gravity (Rees-Sciama effect). A new general numerical method specially designed to estimate these deviations is proposed. It is based on N-body simulations. Using this method, some statistical moments are estimated for the first time.

Quantities Ω and Ω_m are defined as follows: $\Omega = \Omega_b + \Omega_d + \Omega_\Lambda$ and $\Omega_m = \Omega_b + \Omega_d$, where Ω_b, Ω_d and Ω_Λ stand for the density parameters corresponding to baryons, dark matter, and vacuum, respectively. Quantity h is the reduced Hubble constant. We work in the framework of a standard inflationary (flat) model with cold dark matter, having $h = 0.65$, $\Omega_b = 0.05$, $\Omega_d = 0.25$, and $\Omega_\Lambda = 0.7$. The power spectrum has been normalized with $\sigma_8 = 0.93$ according with Eke et al.(1996), who estimated σ_8 to get cluster abundances compatible with observations. In such a model, scalar energy density fluctuations are initially Gaussian, and they remain Gaussian during linear evolution; nevertheless, deviations with respect to Gaussianity arise in the non-linear evolution (where Fourier modes mix).

In this paper, we are concerned with the CMB temperature distribution. This field can be developed in spherical harmonics ($\Delta T/T = \sum_{\ell=0}^{\infty} \sum_{m=-\ell}^{+\ell} a_{\ell m} Y_{\ell m}$). Taking into account the cosmological principle, the CMB temperature is assumed to be a realization of a homogeneous and isotropic statistical field and, as a consequence of this assumption, the m dependence of the bispectrum has –in terms of the Wigner-3j symbols– the well known form :

$$\langle a_{\ell_1 m_1} a_{\ell_2 m_2} a_{\ell_3 m_3} \rangle = B_{\ell_1 \ell_2 \ell_3} \begin{pmatrix} \ell_1 & \ell_2 & \ell_3 \\ m_1 & m_2 & m_3 \end{pmatrix} . \qquad (1)$$

On account of this formula, we can take $m_1 = m_2 = m_3 = 0$ to compute $B_{\ell_1 \ell_2 \ell_3}$ and, then, Eq. (1) allows us to calculate $\langle a_{\ell_1 m_1} a_{\ell_2 m_2} a_{\ell_3 m_3} \rangle$ for other m values. The m dependence of the trispectrum is given explicitly by Hu (2001).

If non-linear evolution is not considered at all, namely, under the assumption that the CMB anisotropy is only produced by linear inflationary fluctuations (which are Gaussian as a result of the generation mechanism), the $a_{\ell m}$ coefficients appear to be statistically independent Gaussian quantities with zero means and variances $\langle \mid a_{\ell m} \mid^2 \rangle = C_\ell$. In this situation (see Grishchuk & Martin 1997), all the odd moments (mean, bispectrum, and so on) vanish, the spectrum is given by $\langle a_{\ell_1 m_1} a_{\ell_2 m_2} \rangle = C_{\ell_1} \delta_{\ell_1 \ell_2} \delta_{m_1,-m_2}$, and the higher order even moments can be written as functions of the C_ℓ quantities , in particular, the relation $\langle \mid a_{\ell m} \mid^4 \rangle = 3C_\ell^2$ is satisfied. In order to test that non-Gaussianity develops during non-linear evolution, deviations with respect to this relation and also with respect to a vanishing bispectrum are investigated.

Along this paper, units are chosen in such a way that the speed of light is $c = 1$ and, whatever quantity "A" may be, $A_{_L}$ and A_0 stand for the A values on the last scattering surface and at present time, respectively.

2 ANGULAR SCALES, BOXES, AND RESOLUTION

We focus our attention on the anisotropy generated while the CMB photons move through the gravitational field produced by non-linear cosmological structures. It is worthwhile to distinguish two types of these structures: (1) mildly non-linear structures having spatial scales larger than those of the clusters (superclusters, voids, Great Attractor-like structures), and (2) strongly non-linear structures with spatial scales either smaller or equal to those of the clusters. In case (1), computations can be performed by using second order perturbation theory as in Mollerach et al. 1995 and Munshi, Souradeep & Starobinski 1995 or, perhaps, the Zel'dovich approach and its generalizations; nevertheless, case (2) requires numerical computations based on N-body schemes. We focus our attention on strongly non-linear structures as clusters, which could produce significant deviations from gaussianity, in particular, during the process of violent relaxation. These structures started to be non-linear (to undergone violent relaxation) at low redshifts of about $z \leq 30$ ($z \leq 3$).

In our flat ΛCDM model, the potential approximation (Martínez-González, Sanz & Silk 1990, 1994; Sanz et al. 1996), can be used to get the following basic equation:

$$\frac{\Delta T}{T} = -\frac{5}{3}\phi_{_L} - \vec{n}\cdot\vec{v}_{_L} - 2\int_{t_{_L}}^{t_o} \vec{\nabla}\phi \cdot d\vec{x} \ , \qquad (2)$$

and

$$\Delta\phi = 4\pi G \delta a^2 \rho_{_B} \ , \qquad (3)$$

where $\frac{\Delta T}{T}$ is the relative temperature variation –with respect to the background temperature– along the direction $\vec{n}$, and the integral is to be computed, from emission at the last scattering surface (L) to observation (O), along the background null geodesics. Symbols x^i ($\vec{x}$), ϕ, $\vec{v}$, $\rho_{_B}$, δ, a, t, G, stand for the comoving coordinates, the peculiar gravitational potential, the peculiar velocity, the background mass density, the density contrast, the scale factor, the cosmological time, and the gravitational constant, respectively. Since we are interested in a gravitational effect, the subdominant baryonic component can be neglected and, consequently, the density contrast – appearing in Eq. (3)– can be evolved using N-body simulations. Our simulations start at $z = 50$ to be sure that all the period of non-linear evolution is taken into account. The Rees-Sciama effect produced by non-linear structures located at redshift $z \leq 50$ is given by the third term of the r.h.s. of Eq. (2), which can be approximated as follows: $\left[\frac{\Delta T}{T}\right]_{_I} \simeq -2\int_{t_{50}}^{t_o} \vec{\nabla}\phi\cdot d\vec{x} \simeq 2\int_{t_{50}}^{t_o} \frac{\partial\phi(\vec{x},t)}{\partial t} dt$, where t_{50} stands for the cosmological time at redshift $z = 50$. Since the anisotropy under consideration can be calculated as an integral of $\partial\phi(\vec{x},t)/\partial t$, the angular scales of this anisotropy are not those subtended by the density contrast itself, but those corresponding to the potential ϕ (see Fullana & Sáez 2000).

The remainder of this section is a qualitative discussion about angular scales and resolution. No accurate computations are necessary and spherically symmetric structures can be considered. According to the cosmological principle, any spherical cosmological structure is compensated at a certain distance or compensation radius $r = \zeta$. The peculiar mass (excess or defect) inside a sphere of radius r, hereafter $M(r)$, vanishes at $r \geq \zeta$ and, taking into account the relation

$$\frac{\partial\phi}{\partial r} \propto \frac{M(r)}{r^2} \ , \qquad (4)$$

which follows from Eq. (3) in the spherically symmetric case, the potential ϕ does not depend on r for $r \geq \zeta$, furthermore, this constant potential must vanishes in order to get a good asymptotic behaviour. This means that a given compensated structure only produces a significant gravitational potential in the region $0 < r < \zeta$; namely, inside a sphere with diameter 2ζ. In the linear regime, the peculiar velocity produced by a structure is $\vec{v} \propto \vec{\nabla}\phi$. Although this relation does not hold in the central non-linear region of a cluster, it roughly holds in the outer regions, where compensation takes place and the density contrast is low. Hence, the peculiar velocity vanishes for $r \geq \zeta$, at the same place where the gravitational potential vanishes by compensation.

If the clustering of clusters is neglected – a good approach in our qualitative analysis– and the present mean separation between neighbouring clusters is ξh^{-1} Mpc, then, the mean distance, at redshift z, is $\xi/(1+z)h$ Mpc and, consequently, given two similar neighbouring clusters, each of them should become roughly compensated at the centre of the segment joining the cluster centres (where peculiar velocity vanishes); therefore, the radius of the region where the potential of a given cluster –at redshift z– is not negligible appears to be $\zeta = \xi/2(1+z)h$. Let us now consider Virgo cluster, which is a standard cluster. It is well known that the peculiar velocity produced by the Virgo cluster on the Local Group ranges between 200 and 300 Km/s; hence, taking into account that the distance from the Local Group to the cluster centre is ~ 20 Mpc ($\sim 13h^{-1}$ Mpc), we can conclude that the Virgo cluster has not been fully compensated at a distance of $\sim 13h^{-1}$ Mpc from its centre. This strongly suggests that, effective compensation should take place between $\zeta = 10h^{-1}$ Mpc ($\xi = 20$) $\zeta = 20h^{-1}$ Mpc ($\xi = 40$); this second value of ζ seems a bit large, although an admissible value in the case of Abell clusters, for which, compensation should be produced at distances greater than those corresponding to Virgo-like structures.

In a flat universe with cosmological constant, the angle

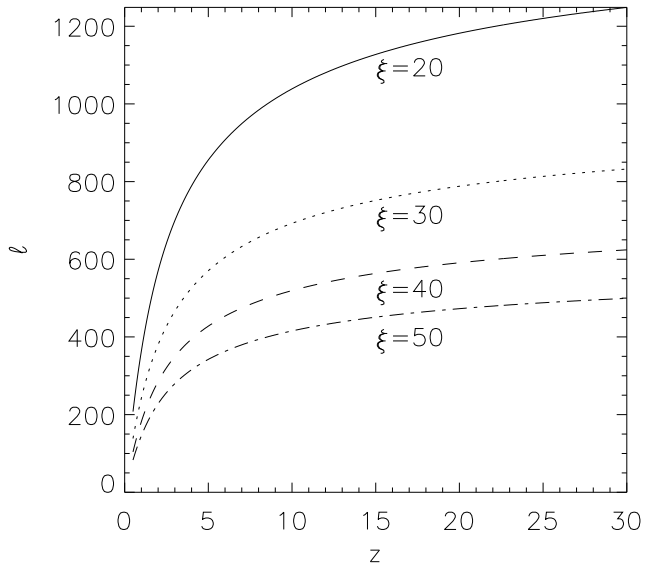

Figure 1. ℓ scale of the non-linear gravitational anisotropy produced by non-linear structures as a function of their redshifts z. Four values of the present scale ξ –defined in the text– are considered.

subtended by the distance $\xi/(1+z)h$ Mpc placed at redshift z is

$$\Delta\theta = \frac{\xi}{3000 f(z)} \tag{5}$$

where

$$f(z) = \int_0^z \frac{d\eta}{[\Omega_{m0}(1+\eta)^3 + \Omega_\Lambda]^{1/2}} \ ; \tag{6}$$

using these formulae, we have calculated the ℓ value corresponding to the angular scale $\Delta\theta$ ($\ell = \pi/\Delta\theta$) as a function of z. The results are displayed in Fig. 1 for $\xi = 20$ (solid line), $\xi = 30$ (dotted line), $\xi = 40$ (dashed line), and $\xi = 50$ (dashed-dotted line). In this Figure we see that, from $z \sim 0.5$ to $z \sim 5$, where clusters undergo violent relaxation and the non-linear gravitational anisotropy should be mainly produced, the ℓ values range in the interval (100,800). For $z < 0.5$, clusters have relaxed and, for $z > 5$, they are at the first stages of their non-linear evolution.

For the sake of briefness and clearness, only the scale $\ell = 400$ (with $m = 0$) has been considered in our calculations. Let us now justify this choice taking into account Fig. 1. The method proposed in this paper might be sensitive to both the degree of non-linearity and the speed of the ϕ evolution. Strong non-linearities and large values of $\partial\phi/\partial t$ (violent relaxation) could lead to numerical problems. Non-linearity requires good spatial resolution in the N-body simulation, and fast ϕ evolution requires appropriate time steps in both the N-body simulation, and the numerical integrations along the line of sight (see below). Fig. 1 shows that non-linear clusters of different sizes located between redshifts 0.5 and 5 (some of them undergoing violent relaxation) are contributing to $\ell = 400$, whereas only small clusters located at $z \sim 5$ (well before violent relaxation) are contributing to $\ell = 800$; therefore, $\ell = 400$ seems to be a good choice in order to test our method taking into account both non-linear evolution and violent relaxation. Moreover, in the model under consideration, the first acoustic peak is located at $\ell = 200$ and, around $\ell = 400$, there is a minimum of the linear dominant Gaussian effects.

Cluster evolution is simulated in boxes having –at present time– 128 Mpc per edge with a resolution of ~ 1 Mpc. This choice is a balance between the need of having a reasonable number of clusters inside the box (order ten) and the need of following the non-linear evolution of the gravitational potential. The minimum scale we resolve, ~ 1 Mpc, is typically of the order of the cluster virial radius and, consequently, non-linear enough. The fine structure within the core cluster is not resolved, but it does not seem to be necessary because the effect under consideration is produced by the gravitational potential, which smoothes all the substructure on the scales we are interested in. The effects produced by substructures ($\xi << 20$ and strong clustering) should appear on angular scales corresponding to $\ell >> 400$, for which more resolution would be necessary.

N-body simulations are performed by using a standard particle-mesh code (Hockney & Eastwood 1988), which was used, tested, and described in more detail by Quilis, Ibañez & Sáez (1998).

We are interested in non-Gaussianity and, consequently, our goal is not the computation of the angular power spectrum (C_ℓ coefficients) corresponding to the third term of Eq. (2). This spectrum was given by Seljak (1996) for the Rees-Sciama effect, and by Fullana & Sáez (2000) for the Integrated Sachs-Wolfe effect. We are looking for the bispectrum, trispectrum and so on. This fact facilitates our implementation of N-body simulations. In the case $\ell = 400$, according to Fig. 1, cluster-like structures ($\xi < 40$) are contributing to the Rees-Sciama effect inside the redshift interval (0.5,5), whereas structures as superclusters, the Great Attractor, and so on ($\xi > 50$), are contributing for $z > 10$, just when they were almost linear objects; hence, these structures can only produce a very small almost Gaussian Integrated effect for $\ell = 400$ (see Fullana & Sáez 2000), and no important deviation from Gaussianity are expected; hence, even if we partially include superclusters and larger structures (small box size), we can get very accurate estimations of the deviations with respect to Gaussianity (associated to strong non-linearity).

Since we are mainly interested in the evolution of the gravitational potential of clusters and substructures and, moreover, the chosen box is much larger than the size of the region where the potential of standard clusters is significant, the Fourier transform can be performed in our box (as it is done in next Section); namely, no important artifacts are expected as a result of the periodicity of an universe filled by boxes identical to the chosen one.

3 DEPARTURES FROM GAUSSIANITY

The basic equations necessary for the numerical computation of the bispectrum and other statistical moments are first derived using the potential approximation and, then, a numerical method for the implementation of these equations –based on N-body simulations– is described and applied.

At present time, the observer is assumed to be located at a certain point with comoving spatial coordinates x_P^i. The equations of the null geodesic passing by point x_P^i are:

$$x^i = x^i_{_P} + \lambda(a) n^i \ , \tag{7}$$

where the function $\lambda(a)$ can be written as follows:

$$\lambda(a) = \kappa(a) H_0^{-1} \ , \tag{8}$$

with

$$\kappa(a) = \int_a^1 \frac{db}{(\Omega_{m0} b + \Omega_\Lambda b^4)^{1/2}} \ . \tag{9}$$

Since we are interested in the deviations from Gaussianity produced by non-linear gravity, the third term of the r.h.s. of Eq. (2) is calculated. Using Eq. (7), this term can be written as follows:

$$\left[\frac{\Delta T}{T}\right]_{_I} (\vec{x}_{_P}, \vec{n}) = \Delta(\vec{x}_{_P}, \vec{n}) = -2 \int_{t_{50}}^{t_o} (\vec{\nabla}\phi \cdot \vec{n}) \dot{\lambda}(a) dt \ , \tag{10}$$

where the dot stands for a time derivative with respect to the cosmological time t.

The following Fourier expansion

$$\phi(\vec{x}, t) = \frac{1}{(2\pi)^{3/2}} \int d^3k e^{-i\vec{k}\cdot\vec{x}} \phi_{\vec{k}}(t) \tag{11}$$

can be combined with Eqs. (7) and (10) to get:

$$\Delta(\vec{x}_{_P}, \vec{n}) = \frac{2i}{(2\pi)^{3/2}} \int_{t_{50}}^{t_o} \dot{\lambda}(t) dt \int d^3k e^{-i\vec{k}\cdot\vec{x}_{_P}} \phi_{\vec{k}}(t) (\vec{k}\cdot\vec{n}) e^{-i\lambda(t)(\vec{k}\cdot\vec{n})} \tag{12}$$

where $\vec{k}$ is the comoving wavevector. Using: (i) Equation (12), (ii) the expansion in spherical harmonics

$$\Delta(\vec{x}_{_P}, \vec{n}) = \sum_{\ell=0}^{\infty} \sum_{m=-\ell}^{+\ell} a_{\ell m}(\vec{x}_{_P}) Y_{\ell m}(\vec{n}) \ , \tag{13}$$

(iii) the identity

$$(\vec{k}\cdot\vec{n}) e^{-i\lambda(t)(\vec{k}\cdot\vec{n})} = 4\pi k \sum_{\ell=0}^{\infty} i^{\ell+1} j'_\ell(\lambda k) \sum_{m=-\ell}^{+\ell} Y_{\ell m}(\vec{n}) Y_{\ell m}(\vec{k}/k), \tag{14}$$

where $j'_\ell(x) = (d/dx) j_\ell(x)$, (iv) the orthonormality relation for the spherical harmonics and (v) the Fourier counterpart of Eq. (3), which reads $\phi_{\vec{k}} = -(D\delta_{\vec{k}})/(ak^2)$, where $D = \frac{3}{2}(1-\Omega_\Lambda) H_0^2 a_0^3$, the following basic equations are easily obtained:

$$a_{\ell m}(\vec{x}_{_P}) = \frac{8\pi D}{(2\pi)^{3/2}} i^\ell \int d^3k e^{-i\vec{k}\cdot\vec{x}_{_P}} k^{-2} Y_{\ell m}(\vec{k}/k) F_\ell(\vec{k}) \tag{15}$$

where

$$F_\ell(\vec{k}) = \int_{w_{50}}^{w_o} f(\vec{k}, w) j'_\ell(w) dw \ , \tag{16}$$

$w = k\lambda(a)$, and $f(\vec{k}, w)$ denotes the function $a^{-1}\delta_{\vec{k}}(a)$ written in terms of the variable w. Eqs. (15) and (16) have been obtained using the Fourier transform in all the space, we have not introduced either boxes or N-body simulations yet. These elements will be only required in order to numerically solve the basic equations (15) and (16).

Evidently, equation (15) can be seen as a Fourier transform from the $\vec{k}$ momentum space to the $\vec{x}_{_P}$ physical space, and the function to be transformed depends on function $F_\ell(\vec{k})$ given by Eq. (16) and other well known functions. In the physical space, each point is the position of a CMB observer who expand the temperature contrast in spherical harmonics to get the coefficients $a_{\ell m}(\vec{x}_{_P})$. From a mathematical point of view (to numerically compute $a_{\ell m}(\vec{x}_{_P})$), we can introduce an appropriate box in physical space with a large enough size (periodic universe). There is another box in momentum space associated to our $\vec{x}_{_P}$ box. In each node of the $\vec{k}$ box, the function $\delta_{\vec{k}}(a)$ must be evaluated a certain number of times to perform the time integral involved in Eq. (16). As it is shown below, this integral can be performed using only the $\delta_{\vec{k}}(a)$ values calculated at each time step by the N-body simulation (see below for details). According to our arguments in Section 2, boxes of 128 Mpc size containing 128^3 observers are appropriate because (a) the resulting function $\delta_{\vec{k}}(a)$ has all the necessary information about non-linearity and (b) periodicity is not expected to be relevant.

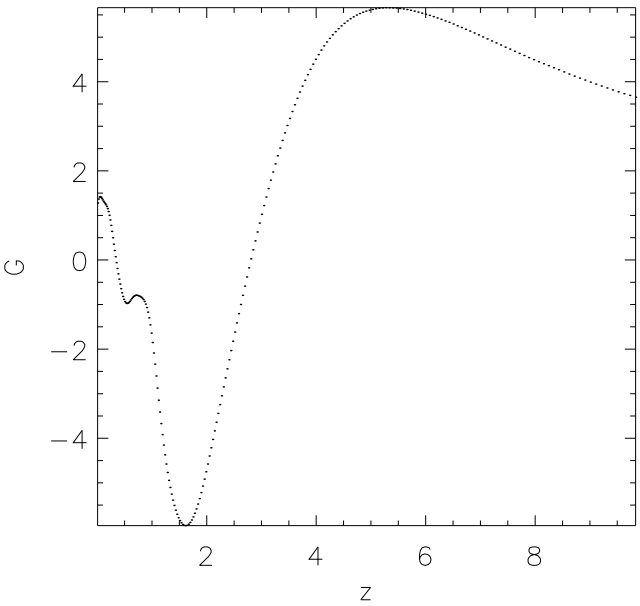

Figure 2. Function $G(z) = f(\vec{k}_0, w(z))$ (see text) for an certain node $\vec{k}_0$ of the computational box. Each point corresponds to a time step of the N-body simulation.

Quantities $a_{\ell m}(\vec{x}_{_P})$ are evaluated on the nodes, $\vec{x}_{_P}$, of the assumed 3D grid as follows: (i) At each time step, t_i, of the N-body simulations (see above), quantity $\delta_{\vec{k}}(a)$ is calculated on the nodes of our 128^3 cubic grid (in momentum space). At a given time t_i, only the quantities $f(\vec{k}, w_{i-1})$ and $f(\vec{k}, w_i)$ are stored, (ii) the integral in Eq. (16) is solved for every node and in each time interval $[t_{i-1}, t_i]$ as it is described below and, then, results from all the time intervals are added to obtain $F_\ell(\vec{k})$. It has been verified that, inside any of the intervals (t_{i-1}, t_i), function $f_i(\vec{k}, w)$ can be very well approximated by a straight line and, as a consequence of this fact, the integral in Eq. (16) can be analytically calculated between t_{i-1} and t_i. The linearity of $f_i(\vec{k}, w)$ is due to the fact that the time step of the N-body simulation is short enough; in order to display this linearity, we present Fig. 2, which shows function $G(z) = f(\vec{k}_0, w(z))$ for a particular node $\vec{k}_0$. Each point is a time step in the N-body simulation and the linear behaviour between contiguous points is evident. The same has been verified for many nodes. From

Fig. 2 it follows that function $f_i(\vec{k},w)$ also has a linear behaviour between more separated points, this fact could be used in future to reduce CPU time; nevertheless, in this paper, linearization is assumed between neighbouring points. The equation of the line joining two neighbouring points

$$f_i(\vec{k},w) = wb_i(\vec{k}) + c_i(\vec{k}) \tag{17}$$

involves two coefficients to be computed from the two stored values $f(\vec{k},w_{i-1})$ and $f(\vec{k},w_i)$. Then, using Eq (17), the value of the integral (16) can be analytically found in any interval $[t_{i-1},t_i]$, the result is

$$F_\ell(\vec{k}) = \sum_i \left[w_i b_i(\vec{k}) + c_i(\vec{k})\right] j_\ell(w_i) - \left[w_{i-1} b_i(\vec{k}) + c_i(\vec{k})\right] j_\ell(w_{i-1}) - b_i(\vec{k}) \int_{w_{i-1}}^{w_i} j_\ell(w)dw \ ; \tag{18}$$

it is noticeable that this formula only involves: the coefficients appearing in Eq. (17), the spherical bessel functions, and the integral of these functions appearing in the last term, and (iii) after computing $F_\ell(\vec{k})$, Eq. (15) –a Fourier transform– is used to obtain $a_{\ell m}(\vec{x}_{_P})$ on the 128^3 nodes of the $\vec{x}_{_P}$ grid. Thus, the expansion in spherical harmonics of the CMB temperature contrasts corresponding to 128^3 observers is obtained and, afterwards, these data are used to perform averages.

Taking into account that $a_{400,0}$ is real, we calculate the i-averages $M^i_{400} = \langle a_{400,0}\rangle$, $C^i_{400} = \langle a^2_{400,0}\rangle$, $B^i_{400} = \langle a^3_{400,0}\rangle$, and $K^i_{400} = \langle a^4_{400,0}\rangle$ over the 128^3 nodes of the i-th simulation. Since these averages have been performed on a limited sample of rather close observers located in a particular region of the universe (nodes in our grid), they appear to change from simulation to simulation. In order to calculate the statistical moments of the CMB, the simulations must be repeated a large enough number of times (to have a big enough sample of CMB observers located in independent regions). Then, the i-averages corresponding to n different simulations ($i = 1, 2, ..., n$) must be averaged again to get the quantities M^n_{400}, C^n_{400}, B^n_{400}, and K^n_{400}, which must tend to the required CMB moments M_{400}, C_{400}, B_{400}, and K_{400}, respectively, as n tends to infinity.

4 DISCUSSION AND RESULTS

In this paper, a new method has been designed with the essential aim of calculating deviations from Gaussianity due to the Rees-Sciama effect. Our method is different from other ones previously used to estimate deviations from Gaussianity due to weak lensing. According to White & Hu (2001), there are too much scales contributing to lensing and *simulating the full range of scales implied is currently a practical impossibility*; sophisticated techniques as "special projections" (Jain, Seljak & White 2000) or "tiling" (White & Hu 2001) have been designed to circumvent the problem; nevertheless, we are not considering lensing here and, as discussed in Section 2, the estimate of the deviations with respect to Gaussianity produced by the Rees-Sciama effect only requires simulations involving a moderated range of scales, which can be performed (see Section 2). In addition, in the Rees-Sciama case, some analytical calculations (Section 3) have given formulae to simultaneously calculate the $a_{\ell m}(\vec{x}_{_P})$ quantities of many observers, from which, the successive statistical moments are calculated by performing appropriate averages.

Condition (17) plays a fundamental role in our numerical method. It leads to Eq. (18), which allows us to compute $F_\ell(\vec{k})$ using a few stored data from the N-body simulation and the spherical Bessel function j_ℓ. This computation of $F_\ell(\vec{k})$ is much faster than any other procedure based on the direct numerical calculation of the integral in Eq. (16). In spite of this fact, the quantities involved in Eq. (18) are (in this paper) evaluated step by step at each node of the computational grid and, consequently, the calculation of $a_{\ell m}(\vec{x}_{_P})$ –although feasible in modern computers– has not a low computational cost. It is worthwhile to remark that, once the quantities $a_{\ell m}(\vec{x}_{_P})$ have been calculated, we can obtain, not only one, but many different moments of the temperature distribution with very small effort (by computing the necessary averages on nodes and realizations).

With the essential aim of finding non-Gaussian features and proving that the proposed method works, we have only considered the case $\ell = 400$, $m = 0$. For very different ℓ values computations would be similar, but the range of spatial scales, the box, and the resolution should be chosen again taking into account Fig. 1. The larger the ℓ value, the greater the necessary resolution. More systematic estimations for other ℓ values –computationally expensive– are in progress. According to some comments in Section 1, the m dependence can be obtained from the results of the m=0 case.

We have performed 90 simulations, in which, the value of $\mid M^i_{400} \mid$ is typically a few times 10^{-19}, whereas about 70% (25%) of the absolute values of $a_{400,0}$ are of the order of 10^{-9} (10^{-10}). This means that –after ensuring the required numerical precision– the positive and negative values of $a_{400,0}$ strongly cancel among them to give a $\mid M^i_{400} \mid$ value as small as reported above. On the contrary, the positive and negative values of $a^3_{400,0}$ (most of them with an absolute value between orders 10^{-27} and 10^{-30}) do not undergo such a strong cancellation, and a significant bispectrum appears (see below).

Quantities C^n_{400}, B^n_{400}, and K^n_{400}, are displayed in Fig. 3 (in terms of the variable n, from $n = 3$ to $n = 90$). As the number of simulations n increases, the values of these quantities should approach the cosmological limit values C_{400}, B_{400}, and K_{400}, respectively. Of course, the three curves in this panel seem to approach constant values as n increases. In order to perform a quantitative study of this behaviour, we have considered the n-interval [20,90], in which all the curves of Fig. 3 seem to approach their limits and, in this interval, we have computed the means and variances of the above n-quantities. Thus, we have found that, within 2σ confidence level, the following relations are satisfied: $C_{400} \times 10^{18} = 1.04 \pm 0.05$, $B_{400} \times 10^{29} = -4.32 \pm 0.27$, $K_{400} \times 10^{36} = 2.45 \pm 0.26$. The mean and variance (from $n = 20$ to $n = 90$) of the quantity $\Gamma^n_{400} = 3(C^n_{400})^2/K^n_{400}$ lead to the following relation $\Gamma_{400} = 1.34 \pm 0.09$, which is valid within 2σ confidence level; therefore, for $\ell = 400$ and $m = 0$, a non-vanishing component of the bispectrum and a non-Gaussian value of the ratio Γ_{400} have been found. It is noticeable the fact that quantities C^n_{400}, B^n_{400}, and K^n_{400} really converge as n increases. There are no uncontrolled er-

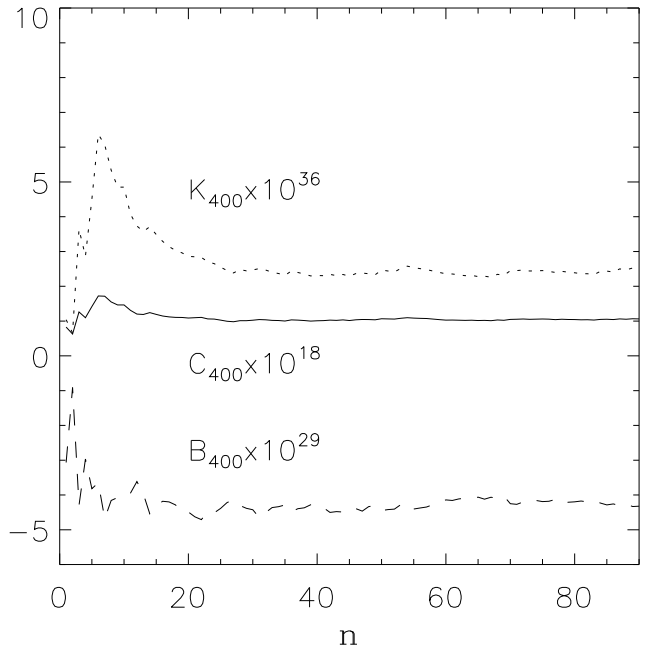

Figure 3. Quantities $C^n_{400} \times 10^{18}$, $B^n_{400} \times 10^{29}$, and $K^n_{400} \times 10^{36}$ vs. the number of simulations n.

rors producing strong oscillations and avoiding convergence, this verification can be seen as a severe test which has been successfully passed by the proposed computational method.

The Rees-Sciama effect was studied by Seljak (1996) in the standard CDM model ($\Lambda = 0$). Four cases corresponding to different values of the parameters σ_8 and $\Omega_{m0}h^2$ were considered by this author, who obtained C_{400} values between 10^{-17} and 10^{-18} corresponding to a signal, $(\Delta T/T)_{rms}$, between 10^{-6} and 10^{-7}. Although we have not computed all the C_ℓ quantities, the resulting C_{400} is comparable to the minimum values obtained by Seljak; hence, the non-linear gravitational effect should be of the order of 10^{-7}, which is below the observational sensitivities of current and planned experiments.

The model of structure formation assumed here is suggested by far supernovae and recent CMB observations. However, other models cannot be ruled out yet. Regardless the structure formation model, our method is ready to do estimations. In any case, our results are challenging to understand the data in forthcoming CMB experiments

ACKNOWLEDGMENTS. This work has been partially supported by the Spanish MCyT (project AYA2000-2045). One of us (VQ) is Marie Curie Research Fellow from the EU (grant HPMF-CT-1999-00052). Calculations were carried out on a SGI Origin 2000s at the Centro de Informática de la Universitat de València.

REFERENCES

Eke V., Cole S., Frenk C.S., 1996, MNRAS, 282, 263
Fullana M.J., Sáez D., 2000, New Astronomy, 5, 109
Grishchuck L.P., Martin J., 1997, Phys. Rev., 56D, 1924
Hockney R.W., Eastwood J.W., 1988, Computer Simulations Using Particles (Bristol: IOP Publishings)
Hu W., The Angular Trispectrum of the CMB, astro-ph/0105117
Jain B., Seljak U., White S., 2000, ApJ, 530, 547
Martínez-González E., Sanz J.L., Silk J., 1990, ApJ, 355, L5
Martínez-González E., Sanz J.L., Silk J., 1994, ApJ, 436, 1
Mollerach S., Gangui A., Lucchin F., Matarrese S., 1995, ApJ, 453, 1
Munshi D., Souradeep T., Starobinski A. A., 1995, ApJ, 454, 552
Quilis V., Ibáñez J.M., Sáez D., 1998, ApJ, 502, 518
Sanz J.L., Martínez-González, E., Cayón L., Silk J.L., Sugiyama N., 1996, ApJ, 467, 485
Seljak U., 1996, ApJ, 460, 549
Tuluie R., Laguna P., Anninos P., 1996, ApJ, 463, 15
White M., Hu W., 2000, ApJ, 537, 1